Hindawi
Advances in Multimedia
Volume 2022, Article ID 2133735, 14 pages
https://doi.org/10.1155/2022/2133735

Research Article

Verification of the Improvement Effect of Artificial Intelligence Computer Control Technology on Electrical Automation Control

Jinpeng Li

School of Mathematics and Information, Xinyang Vocational and Technical College, Xinyang 464000, China

Correspondence should be addressed to Jinpeng Li; ljp@xyvtc.edu.cn

Received 27 May 2022; Revised 15 August 2022; Accepted 23 August 2022; Published 15 September 2022

Academic Editor: Qiangyi Li

Copyright © 2022 Jinpeng Li. This is an open access article distributed under the Creative Commons Attribution License, which permits unrestricted use, distribution, and reproduction in any medium, provided the original work is properly cited.

In order to improve the effect of electrical automation control, this paper combines the intelligent computer technology to construct the electrical automation control system, explores the principle of the active disturbance rejection controller, and applies it to the induction motor vector control system. The active disturbance rejection controller estimates the state variables of the system and their changing trends in real time through the extended state observer, compensates them by nonlinear feedback method, and provides appropriate control signals. In addition, this paper builds the induction motor active disturbance rejection control system based on ant colony algorithm and conducts a lot of simulation analysis. The research shows that the electrical automatic control system based on the intelligent computer algorithm proposed in this paper has a good electrical automatic control effect.

1. Introduction

Industrial Control Computer is also referred to as IPC. In the field of industrial control, the computer has also been applied, which is the so-called industrial PC. Because the application environment of industrial computers is industrial control, industrial computers are different from ordinary computers and have their own unique characteristics [1]. Moreover, due to the different performance requirements of different uses, industrial computers have wider requirements for working temperature. In addition, industrial computers have better performance in terms of dustproof, antivibration and anti-interference.

IPC does not pursue extreme hardware performance requirements, as long as it is sufficient to meet the control requirements; hardware stability is the key to IPC, which is much higher than that of ordinary computers [2].

The power system consists of three parts: the power source, the power network, and the load. Electric energy generated by power generation equipment is transmitted to users through the power network [3]. The natural gas system mainly includes natural gas pipelines, compressor stations, pressure regulating valves, and valves. Natural gas is input into pipelines from supply sources, and then, transported to users through the natural gas pipeline network. The pressure regulating valve is mainly used to control the pressure of different nodes in the natural gas pipeline network, and the natural gas flow can be adjusted by changing the position of the valve spool [4]. The integrated energy system of electrical interconnection is formed by coupling gas turbines and P2G equipment. At present, in the planning and operation of the electrical interconnection system, there are not many studies on the location and capacity of P2G equipment and gas turbine units [5]. The operation planning of the electrical interconnection system usually takes the coordinated operation of each subsystem as the planning premise, considers the respective operational constraints of the electrical system, and then designs the objective function that minimizes the sum of the investment cost and the operating cost to complete the modeling of the electrical interconnection system. [6].

The so-called configuration software is actually a software system that communicates with the control system and is responsible for the real-time data acquisition and monitoring of the system. The English abbreviation of configuration software is SCADA, which means monitoring

and data acquisition [7]. Configuration software first originated from industrial control computers. The communication function of configuration software is very powerful, almost all control devices can find configuration software that can communicate with it, which makes the application range of configuration software very wide, configuration software allows users to customize the interface of the control system, and can create complex configuration software. The dynamic monitoring screen of the real-time control system, completes the real-time monitoring of the process of the control system through real-time communication connection, and has functions such as alarming, recording historical data, and simulation [8]. The so-called field bus is actually a network, which connects field devices, field controllers, sensors, various terminals, etc., and realizes fast, efficient, regulated, reliable, and simple field data exchange through certain standard communication methods or pass [9]. Full digitization is one of the characteristics of fieldbus control technology. The wiring rules of fieldbus technology are very simple. Under the master control system, the master device only needs to lead out a cable, connect it to the input end of the fieldbus slave device, and then, connect the output end of the slave device to the next bus slave. The input terminal of the station device, connect all the slave devices in turn [10]. Now there are many programmable controllers with fieldbus master control functions, which can easily form a system with bus-type control equipment, making the wiring, installation and maintenance of the system more concise, reducing costs, improving stability, and simplifying program development [11]. The motion controller is the core control device for the servo drive, which can realize multiaxis motion control by connecting multiple sets of servo systems. Different from the pulse control method of the traditional servo system, the current mainstream motion controller adopts the field bus structure, which can make the entire servo control system faster and more reliable, and at the same time, the wiring is simpler and easier to expand [12]. Common international standard field buses are CANopen bus, PPROFIBUS bus, EtherCAT bus, and SERCOS bus. Bus-type motion controllers are generally embedded with multiaxis motion control functions such as electronic cams, flying shears, and virtual axes. Of course, they can also realize single-axis speed and position control, which has wide application value in multiaxis motion control occasions.

The electrical automatic control system of the industrial production process is an indispensable basic production facility in various fields, and its core is the electric drive technology and digital control technology. With the high development of computer technology, transmission control technology, and high-power industrial electronic technology, AC electric transmission control technology has now developed to a relatively mature stage [13]. Compared with more traditional electrical equipment such as DC motors, the advantages of AC motor equipment are high single-unit capacity (kVA), low rotational transmission inertia, high transmission efficiency, and optimized structure, wide performance adjustment range and reliable operation. After years of development, the performance of AC drive equipment has surpassed the typical performance of DC drive equipment at many levels. There is a rapid development trend of generally adopting AC drive equipment to replace the previous DC drive equipment [14]. In terms of the main equipment and auxiliary electric drive of the mechanical product production line, developed countries have taken the lead in replacing the DC system with AC speed control equipment.

The design of the host control system station, hereinafter referred to as the master station, should be based on intrinsically safe PLC, and then, start to select other hardware, including power modules and host computers; the selected hardware must be able to meet the basic functional requirements, and must have extended The basic requirements are to have a display interface, a control interface, the display interface includes monitoring and dynamic analysis, and the control interface has basic buttons, indicator lights, etc. [15]. The design of the slave control system station, hereinafter referred to as the slave station, the most important thing for the slave station is to collect data, analyze the data, and send the results to the master station, and it must have a distinguishing function itself. In the local situation, there must be automatic control features. For the realization of this series of functions, the selection of sensor hardware is particularly important. It is related to whether the fault can be checked, directly related to the stability and reliability of the function, and even related to the quality of the product. Therefore, the selection of sensors should be considered comprehensively. Starting from its own stability, reliability, power supply, data acquisition accuracy, etc. [16]; in addition to sensors, there must be special requirements for the customization of the control cabinet, because there is a pressure difference in the mine, the selection of the control cabinet is also a challenge [17].

The traditional ADRC has a defect; that is, the control effect is directly related to the selection of the internal parameters of the controller, and according to the different controlled objects, the direction and size of the parameter setting are uncertain, which makes the parameter setting difficult and limits the automatic control of popularization and practicability of disturbance rejection controller.

In order to improve the dynamic performance of the speed control system, this paper introduces the active disturbance rejection technology into the induction motor vector control system, trying to reduce the dependence of the traditional controller design on the controlled object and overcome the disadvantages of the controlled motor parameter change, modeling error, and load disturbance. The core of ADRC is to regard the unmodeled dynamics and unknown external disturbance of the system as the "total disturbance" of the system and to estimate and compensate accordingly.

The ant colony algorithm is used as a parameter optimization mechanism, and is added to the induction motor ADRC control system based on ADRC. Using the distributed search and parallel computing capabilities of the ant colony algorithm, the induction motor ADR control system based on the ant colony algorithm has the self-learning ability of automatic parameter optimization.

This paper builds the induction motor active disturbance rejection control system based on ant colony algorithm, and conducts a lot of simulation analysis.

2. Design of Electrical Automation Control System

In the process of electrical automation control, the electrical function structure analysis is carried out through intelligent modeling, and the electrical automation control model is modeled and analyzed below.

2.1. Introduction to the System Principle of Induction Motor Vector Control. The induction motor is an indispensable part of the electrical automation control system, and the model of this part is modeled first.

When the mathematical model of the induction motor is established, some necessary and reasonable simplifying assumptions are often made for the convenience of analysis:

(1) The magnetic circuit is not saturated, and there is no adverse effect of hysteresis and eddy current. The skin effect generated by high-frequency current in the iron core and the wire is ignored, and the temperature rise and skin effect are ignored, which leads to the change of winding resistance

(2) The magnetic circuit of the motor is linear, and the self-inductance and mutual inductance of the motor remain constant

(3) The straight axis and the quadrature axis in the motor structure are strictly vertical according to the standard

(4) The magnetic potential is sinusoidally distributed

The three-phase induction motor model is shown in Figure 1.

The voltage equation of the three-phase stator winding is

$$\begin{aligned} u_A &= i_A R_s + \frac{d\psi_A}{dt}, \\ u_B &= i_B R_s + \frac{d\psi_B}{dt}, \\ u_C &= i_C R_s + \frac{d\psi_C}{dt}. \end{aligned} \tag{1}$$

In the same way, the voltage equation after the three-phase rotor winding is converted to the stator side is

$$\begin{aligned} u_a &= i_a R_r + \frac{d\psi_a}{dt}, \\ u_b &= i_b R_r + \frac{d\psi_b}{dt}, \\ u_c &= i_c R_r + \frac{d\psi_c}{dt}. \end{aligned} \tag{2}$$

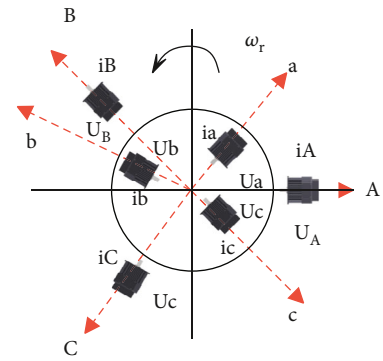

Figure 1: Three-phase induction motor model.

Therefore, the voltage equation in matrix form is

$$\begin{pmatrix} U_A \\ U_B \\ U_C \\ U_a \\ U_b \\ U_c \end{pmatrix} = \begin{pmatrix} R_S & 0 & 0 & 0 & 0 & 0 \\ 0 & R_S & 0 & 0 & 0 & 0 \\ 0 & 0 & R_S & 0 & 0 & 0 \\ 0 & 0 & 0 & R_r & 0 & 0 \\ 0 & 0 & 0 & 0 & R_r & 0 \\ 0 & 0 & 0 & 0 & 0 & R_r \end{pmatrix} \begin{pmatrix} i_A \\ i_B \\ i_C \\ i_a \\ i_b \\ i_c \end{pmatrix} + \frac{d}{dt} \begin{pmatrix} \Psi_A \\ \Psi_B \\ \Psi_C \\ \Psi_a \\ \Psi_b \\ \Psi_c \end{pmatrix}. \tag{3}$$

The flux linkage is the sum of the self-induction flux linkage and the mutual induction flux linkage. Therefore, the flux linkage equation is

$$\begin{pmatrix} \Psi_A \\ \Psi_B \\ \Psi_C \\ \Psi_a \\ \Psi_b \\ \Psi_c \end{pmatrix} = \begin{pmatrix} L_{AA} & L_{AB} & L_{AC} & L_{Aa} & L_{Ab} & L_{Ac} \\ L_{BA} & L_{BB} & L_{BC} & L_{Ba} & L_{Bb} & L_{Bc} \\ L_{CA} & L_{CB} & L_{CC} & L_{Ca} & L_{Cb} & L_{Cc} \\ L_{aA} & L_{aB} & L_{aC} & L_{aa} & L_{ab} & L_{ac} \\ L_{bA} & L_{bB} & L_{bC} & L_{ba} & L_{bb} & L_{bc} \\ L_{cA} & L_{cB} & L_{cC} & L_{ca} & L_{cb} & L_{cc} \end{pmatrix} \begin{pmatrix} i_A \\ i_B \\ i_C \\ i_a \\ i_b \\ i_c \end{pmatrix}. \tag{4}$$

In the formula, L is the 6×6 inductance matrix. L_{AB} LAB represents the mutual induction between A and B and other analogies.

The magnetic flux of a certain phase winding of the motor includes the leakage flux that does not pass through the air gap. The other type is the mutual induction flux passing through the air gap, and the mutual induction magnetic flux dominates.

The flux linkage equation (4) is substituted into the voltage equation (3) to obtain the voltage equation:

$$\begin{aligned} u = Ri + p(Li) = Ri + L(di/dt) + (dL/dt)i == Ri + L(di/dt) \\ + (dL/d\theta)\omega_r i. \end{aligned} \tag{5}$$

In the formula, $L(di/dt)$ belongs to the pulsating electromotive force in the electromagnetic induction electromotive force, and $(dL/d\theta)\omega_r i$ belongs to the rotating electromotive force that is proportional to ω_r in the electromagnetic induction electromotive force.

The equation of motion of the motor is

$$T_e = T_L + \frac{J}{P_n}\frac{d\omega_r}{dt} + \frac{\eta}{P_n}\omega_r. \tag{6}$$

According to the principle of electromechanical energy conversion, the electromagnetic torque of the three-phase asynchronous motor can be obtained as:

$$\begin{aligned} T_e = P_n L_m[&(i_A i_a + i_B i_b + i_C i_c)\sin\theta + (i_A i_b + i_B i_c + i_C i_a)\sin(\theta + 120^\circ) \\ &+ (i_A i_c + i_B i_a + i_C i_b)\sin(\theta - 120^\circ)]. \end{aligned} \tag{7}$$

That is, the drag torque is a multivariable, nonlinear and strongly coupled function.

Equation Formulas (4), (5), (6), (7) are summed up to form the mathematical model of the three-phase induction motor in the ABC coordinates.

2.2. Coordinate Transformation Matrix. For the electrical automation control system, the coordinate transformation matrix is the control core algorithm of the overall model. In this paper, the series control of each functional structure is realized through the coordinate transformation matrix.

The research method of coordinate transformation is used to convert i_A, i_B, i_C in the three-phase static coordinate system to i_α, i_β in the two-phase static coordinate system, and further convert it into i_d, i_q in any two-phase rotating coordinate system, and mutual conversion in the three coordinate systems. It is easy to analyze and control the induction motor through the transformation of the coordinate system. The transformation matrix $C_{3s/2s}$ for converting the three-phase stationary coordinate system to the two-phase stationary coordinate system is

$$C_{3s/2s} = \sqrt{\frac{2}{3}}\begin{bmatrix} 1 & \frac{-1}{2} & \frac{-1}{2} \\ 0 & \sqrt{\frac{3}{2}} & -\sqrt{\frac{3}{2}} \end{bmatrix}. \tag{8}$$

That is,

$$\begin{bmatrix} i_\alpha & i_\beta \end{bmatrix}^T = C_{3s/2s}\begin{bmatrix} i_A & i_B & i_C \end{bmatrix}^T. \tag{9}$$

Its inverse transformation matrix $C_{2\,s/3s}$ is

$$C_{2s/3s} = \sqrt{\frac{2}{3}}\begin{bmatrix} 1 & 0 \\ -1/2 & \sqrt{3}/2 \\ -1/2 & -\sqrt{3}/2 \end{bmatrix}. \tag{10}$$

That is

$$\begin{bmatrix} i_A & i_B & i_C \end{bmatrix}^T = C_{2s/3s}\begin{bmatrix} i_\alpha & i_\beta \end{bmatrix}^T. \tag{11}$$

The transformation matrix $C_{2s/2r}$ from the two-phase stationary coordinate system to the two-phase rotating coordinate system is

$$C_{2s/2r} = \begin{bmatrix} \cos\phi & \sin\phi \\ -\sin\phi & \cos\phi \end{bmatrix}. \tag{12}$$

That is.

$$\begin{bmatrix} i_d & i_q \end{bmatrix} = C_{2s/2r}\begin{bmatrix} i_\alpha & i_\beta \end{bmatrix}^T. \tag{13}$$

Its inverse transformation matrix $C_{2r/2s}$ is

$$C_{2r/2s} = \begin{bmatrix} \cos\phi & -\sin\phi \\ \sin\phi & \cos\phi \end{bmatrix}. \tag{14}$$

That is

$$\begin{bmatrix} i_\alpha & i_\beta \end{bmatrix}^T = C_{2r/2s}\begin{bmatrix} i_d & i_q \end{bmatrix}^T. \tag{15}$$

The transformation matrix $C_{35/2r}$ for converting the three-phase stationary coordinate system to the two-phase rotating coordinate system is:

$$C_{3s/2r} = \sqrt{\frac{2}{3}}\begin{bmatrix} \cos\varphi & \cos(\varphi - 120^\circ) & \cos(\varphi + 120^\circ) \\ \sin\varphi & \sin(\varphi - 120^\circ) & \sin(\varphi + 120^\circ) \end{bmatrix}. \tag{16}$$

That is,

$$\begin{bmatrix} i_d & i_q \end{bmatrix}^T = C_{3s/2r}\begin{bmatrix} i_A & i_B & i_C \end{bmatrix}^T. \tag{17}$$

Its inverse transformation matrix $C_{2r/3s}$ is

$$C_{2r/3s} = \sqrt{\frac{2}{3}}\begin{bmatrix} \cos\phi & -\sin\phi \\ \cos(\phi - 120^\circ) & -\sin(\phi - 120^\circ) \\ \cos(\phi + 120^\circ) & -\sin(\phi + 120^\circ) \end{bmatrix}. \tag{18}$$

This paper chooses the multi-Lyapunov energy function method, which can reduce the conservativeness of the conclusions of this paper. Compared with the general single Lyapunov function method, this method has better performance and is more flexible. The multi-Lyapunov function method can be described by the following mathematical formula:

$$V_{\sigma(t),\delta(t)}(t) = \xi^T(t)P_{\sigma(t),\delta(t)}\xi(t), \tag{19}$$

where $V_{i,0}(t)$ and $V_{i,1}(t)$ correspond to the energy subfunction of the i subsystem.

This form of Lyapunov function expression, with most existing ones having only one corresponding energy function for all subsystems, our results will be less conservative. Lyapunov functions of the above form are called multiple Lyapunov functions. For such a Lyapunov function, the following assumption is usually made: at the switching moment, the energy function is abruptly upwards. Therefore, to ensure the stable state of the entire switching system is to ensure that in the process of multiple switching, even if the switching energy increases each time, the stable state of the entire event-triggered switching system is achieved by restricting the model-dependent dwell time.

Suppose the ith subsystem is active for model-dependent dwell time $[t_i, t_{i+1})$ and the j-th subsystem is active for model-dependent dwell time $[t_{i-1}, t_i)$. For a given scalar $u_i > 1, 0 < v_i < 1, t_k$ and $u_i > 1, 0 < v_i < 1, t_k$ represent the sample point, $t_i + T_\sigma$ represents another switching point in the switching interval $[t_i, t_{i+1})$. According to the above assumptions, the corresponding mathematical models are

$$\begin{aligned}
&\iota_1 ||x(t)||^2 \le V_{\sigma(t),\delta(t)}(t) \le \iota_2 ||x(t)||^2,\\
&\dot{V}_{\sigma(t),\delta(t)}(t) \le -a_{\sigma(t),\delta(t)} V_{\sigma(t),\delta(t)}(t) - \Gamma(t),\\
&t \in S_1, S_2 = \{t | \forall t \in (t_k, t_{i+1}), t_k \in [t_k, t_{i+1})\},\\
&\dot{V}_{\sigma(t),0}(t) \le -a_{\sigma(t),1} V_{\sigma(t),0}(t) - \Gamma(t),\\
&t \in S_1, S_2 = \{t | \forall t \in (t_i, t_k), t_i < t_k\},\\
&\dot{V}_{\sigma(t),\delta(t)}(t) \le \beta_{\sigma(t)} V_{\sigma(t),\delta(t)}(t) - \Gamma(t), t \notin S_1 \cup S_2,\\
&V_{\sigma(t),1}(t_i + T_\sigma) \le v_\sigma(t) V_{\sigma(t),0}((t_i + T_\sigma)^-),\\
&V_{\sigma(t),0}(t_i) \le \mu_\sigma(t) V_{\sigma(tj),1}(t_i^-),\\
&\Gamma = e^T(t) e(t) - \gamma^2 \tilde{\omega}^T(t) \tilde{\omega}(t).
\end{aligned} \tag{20}$$

The flux linkage equation in the two-phase stationary coordinate $\alpha\beta$ is

$$\psi_{s\alpha} = L_s i_{s\alpha} + L_m i_{r\alpha}, \tag{21}$$

$$\psi_{s\beta} = L_s i_{s\beta} + L_m i_{r\beta}, \tag{22}$$

$$\psi_{r\alpha} = L_m i_{s\alpha} + L_r i_{r\alpha}, \tag{23}$$

$$\psi_{r\beta} = L_m i_{s\beta} + L_r i_{r\beta}. \tag{24}$$

The voltage equation is

$$\begin{bmatrix} u_{s\alpha} \\ u_{s\beta} \\ u_{r\alpha} \\ u_{r\beta} \end{bmatrix} = \begin{bmatrix} R_s + L_s p & 0 & L_m p & 0 \\ 0 & R_s + L_s p & 0 & L_m p \\ L_m p & \omega_r L_m & R_r + L_r p & \omega_r L_r \\ -\omega_r L_m & L_m p & -\omega_r L_r & R_r + L_r p \end{bmatrix} \begin{bmatrix} i_{s\alpha} \\ i_{s\beta} \\ i_{r\alpha} \\ i_{r\beta} \end{bmatrix}. \tag{25}$$

The torque equation is

$$T_e = p_n L_m \left(i_{s\beta} i_{r\alpha} - i_{s\alpha} i_{r\beta} \right). \tag{26}$$

The formula (21), formula (25), and formula (26) are combined to form the mathematical model of the induction motor in the two-phase stationary $\alpha\beta$ coordinate system.

Stator current and rotor flux linkage are selected as the state of induction motor electromagnetic system, $x = \begin{bmatrix} i_{sd} & i_{sq} & \psi_{rd} & \psi_{rq} \end{bmatrix}^T$. The stator voltage is taken as the control variable, $u = \begin{bmatrix} u_{sd} & u_{sq} \end{bmatrix}^T$.The following state equation can be sorted out:

$$\begin{bmatrix} \dot{i}_{sd} \\ \dot{i}_{sq} \\ \dot{\psi}_{rq} \\ \dot{\psi}_{rd} \end{bmatrix} = \begin{bmatrix} -\left(\frac{R_s}{\delta L_s} + \frac{1-\delta}{\delta \tau_r}\right) & \omega_c & \frac{L_m}{\delta L_s L_r \tau_r} & \omega_c \frac{L_m}{\delta L_s L} \\ -\omega_c & -\left(\frac{R_s}{\delta L_s} + \frac{1-\delta}{\delta \tau_r}\right) & -\omega_r \frac{L_m}{\delta L_s L} & \frac{L_m}{\delta L_s L_r \tau_r} \\ \frac{L_m}{\tau_r} & 0 & -\frac{1}{\tau_r} & (\omega_c - \omega_r) \\ 0 & \frac{L_m}{\tau_r} & -(\omega_c - \omega_r) & -\frac{1}{\tau_r} \end{bmatrix} \begin{bmatrix} i_{sd} \\ i_{sq} \\ \psi_{rq} \\ \psi_{rd} \end{bmatrix} + \begin{bmatrix} \frac{1}{\delta L_s} & 0 \\ 0 & \frac{1}{\delta L_s} \\ 0 & 0 \\ 0 & 0 \end{bmatrix} \begin{bmatrix} u_{sd} \\ u_{sq} \end{bmatrix}. \tag{27}$$

2.3. Structure and Principle of Active Disturbance Rejection Controller. There are linear and nonlinear control methods for the control of the AD process. In this paper, the nonlinear tracking method is selected to model the system to realize the intelligent control of the input and output signals.

The running time of all mismatches of the filter satisfies inequality

$$\tilde{T} < \frac{\lambda - \breve{\lambda}}{\tilde{\lambda} - \lambda} \breve{T} + \frac{\lambda - \widehat{\lambda}}{\tilde{\lambda} - \lambda} \widehat{T}. \tag{28}$$

Among,

$$\begin{aligned}\breve{\lambda} &= \max_{i\in L}\left\{\ln \mu_i/\tau_i + \ln \nu_i/\tau_i - a_{i,0}\right\},\\ \widehat{\lambda} &= \max_{i\in \tau}\left\{\ln \nu_i/\tau_i - a_{i,1}\right\},\\ \tilde{\lambda} &= \max_{i\in \tau}\left\{\ln \nu_i/\tau_i + \beta_i\right\},\end{aligned} \tag{29}$$

and $\breve{\lambda}, \widehat{\lambda}, \tilde{\lambda}$ satisfies inequality:

$$\max\left\{\breve{\lambda}, \widehat{\lambda}, \tilde{\lambda}\right\} < \lambda < 0. \tag{30}$$

Then, the filter error system is GUES.

Consider $t \in (t_i + T_\sigma, t_{i+1}), i \in \tau$,

$$\begin{aligned}V_{\sigma(t_i)}(t) &\le \nu^{T_i} \exp\left(-a_{i,0}\breve{T}_i - a_{i,1}\widehat{T}_i + \beta_i\tilde{T}_i\right)V_{\sigma(t_i)}(t_i) - \nu_i^{T_i}\int_{t_i}^{t}\\ &\exp\left(-a_{i,0}\breve{T}_i - a_{i,1}\widehat{T}_i + \beta_i\tilde{T}_i\right)\Gamma(s)ds \le \mu_i\nu_i^{T_i}\\ &\exp\left(-a_{i,0}\breve{T}_i - a_{i,1}\widehat{T}_i + \beta_i\tilde{T}_i\right)V_{\sigma(t_j)}(t_i^-) - \mu_i\nu_i^{T_i}\int_{t_i}^{t}\\ &\exp\left(-a_{i,0}\breve{T}_i - a_{i,1}\widehat{T}_i + \beta_i\tilde{T}_i\right)\Gamma(s)ds\cdots \le \prod_{i\in\tau}\mu_i^N\nu_i^{T_i}\\ &\exp\left(-a_{i,0}\breve{T}_i - a_{i,1}\widehat{T}_i + \beta_i\tilde{T}_i\right)V_{\sigma(t_0)}(t_0) - \sum_{t_\theta=t_0}^{t_{i-1}}\mu_i^{N(t_\theta=t_0)}\nu_i^{T_i(t_\theta=t_0)}\\ &\times \exp\left(-a_{i,0}\theta_{a_{i,0}}(t_\theta=t) + a_{i,1}\theta_{a_{i,1}}(t_\theta=t) + \beta_{i,0}\theta_{\beta_i}(t_\theta=t)\right)\\ &\times \exp\int_{t_\theta}^{t_\theta+1}\exp\left(-a_{i,0}\breve{T}_i - a_{i,1}\widehat{T}_i + \beta_i\tilde{T}_i\right)\Gamma(s)ds.\end{aligned} \tag{31}$$

If $\omega(t) = 0$, then $\Gamma(t) > 0$, inequality holds

$$\begin{aligned}V_{\sigma(t_i)}(t) &< \prod_{i\in\tau}\mu_i^N\nu_i^{T_i}\exp\left(-a_{i,0}\breve{T}_i - a_{i,1}\widehat{T}_i + \beta_i\tilde{T}_i\right)V_{\sigma(t_0)}(t_0)\\ &\cdot \le \prod_{i\in\tau}\mu_i^{T_i/\tau_i}\nu_i^{\breve{T}_i/\tau_i}\exp\left(-a_{i,0}\breve{T}_i - a_{i,1}\widehat{T}_i + \beta_i\tilde{T}_i\right)V_{\sigma(t_0)}(t_0)\\ &\cdot \le \prod_{i\in\tau}\exp\left((T_i/\tau_i)\ln\mu_i + \left(\breve{T}_i/\tau_i\right)\ln\nu_i - a_{i,0}\breve{T}_i - a_{i,1}\widehat{T}_i + \beta_i\tilde{T}_i\right)\\ &\cdot \times V_{\sigma(t_0)}(t_0).\end{aligned} \tag{32}$$

By inequalities (28) and (29), we get

$$\begin{aligned}V_{\sigma(t_i)}(t) &\le \exp\left(\breve{T}\breve{\lambda} + \widehat{T}\widehat{\lambda} + \tilde{T}\tilde{\lambda}\right)V_{\sigma(t_0)}(t_0)\\ &\le \exp\left(\lambda(t-t_0)\right)V_{\sigma(t_0)}(t_0),\end{aligned} \tag{33}$$

where $t \longrightarrow 0$ and $V_{\sigma(t_0)}(t_0)$ converges to 0.

Feed it a signal $v(t)$ and it will give two outputs $x_1(t)$ and $x_2(t)$, where $x_1(t)$ tracks the input signal and $x_2(t)$ is the differential of $x_1(t)$. $x_2(t)$ is actually the generalized differential of $v(t)$.

According to the capacity of the object, a reasonable transition process $x_1(t)$ is arranged, which is also a way to improve the robustness of the regulator.

The system is considered as:

$$\dot{x}_1 = x_2, \tag{34}$$

$$\dot{x}_2 = f(x_1, x_2, t) + b\cdot u, \tag{35}$$

$$y = x_1. \tag{36}$$

If $f(x_1, x_2, t)$ is known, its observer can be designed as:

$$\varepsilon_1 = z_1 - y, \tag{37}$$

$$\dot{z}_1 = z_2 - \beta_1\cdot\varepsilon_1, \tag{38}$$

$$\dot{z}_2 = f(z_1, z_2, t) - \beta_2\cdot\varepsilon_1 + b\cdot u. \tag{39}$$

However, in many cases, $f(x_1, x_2, t)$ is not known, and when $f(x_1, x_2, t)$ is not known, $f(x_1, x_2, t)$ is regarded as a disturbance. We set $x_3 = f(x_1, x_2, t), \dot{x}_3 = g(x_1, x_2, t)$, then, $g(x_1, x_2, t)$ is also an unknown function, so the system equation becomes

$$\begin{aligned}\dot{x}_1 &= x_2,\\ \dot{x}_2 &= x_3 + b\cdot u,\\ \dot{x}_3 &= g(x_1, x_2, t),\\ y &= x_1.\end{aligned} \tag{40}$$

The corresponding state observer becomes

$$\begin{aligned}\varepsilon_l &= z_l(k) - y(k),\\ \dot{z}_l(k+l) &= z_l(k) + T\cdot(z_2(k) - \beta_l\cdot\varepsilon_l),\\ \dot{z}_2 &= z_3 - \beta_2\cdot\mathrm{fal}(\varepsilon_l, \alpha_1, \delta) + b\cdot u,\\ \dot{z}_3 &= -\beta_3\cdot\mathrm{fal}(\varepsilon_1, \alpha_2, \delta).\end{aligned} \tag{41}$$

Among them, there is

$$\mathrm{fal}(\varepsilon, \alpha, \delta) = \begin{cases}|\varepsilon|^\alpha\cdot\mathrm{sign}\ (\varepsilon), |\varepsilon| > \delta,\\ \varepsilon\cdot\delta^{\alpha-1}, |\varepsilon| \le \delta.\end{cases} \tag{42}$$

The expanded state z_3 can make a good estimate of the "real-time effect" $f(x_1, x_2, t)$ of the "unknown perturbation". Therefore, the system (37) is referred to as the extended state observer of the system (34).

The use of nonlinear feedback has many efficient properties:

For a first-order error system, there is

$$\frac{de}{dt} = w + u. \tag{43}$$

(1) We use the linear feedback $u = -k\cdot e, k > 0$ of the error to the system, then, we have

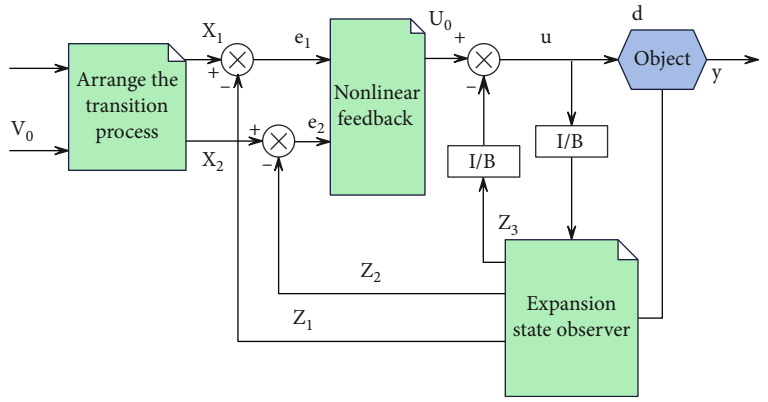

Figure 2: Structure diagram of the second-order ADRC controller.

$$\frac{de}{dt} = -k \cdot e + w, \frac{1}{2}\frac{de^2}{dt} + k \cdot e = e \cdot w. \tag{44}$$

If there is a constant w_0 greater than zero that satisfies $|w| < w_0$, there is

$$\frac{1}{2}\frac{de^2}{dt} < -k \cdot |e|(|e| - w_0/k). \tag{45}$$

When there is $|e| > w_0/k$, there is $de^2/dt < 0$; that is, the steady-state error of the system is less than w_0/k, and the steady-state error is inversely proportional to the feedback gain k under linear feedback conditions.

(2) We use the nonlinear feedback $u = -k \cdot |e|^{\alpha} \cdot \text{sign}\,(e)$, $\alpha > 0$ of the error to the system, then, we have

$$\frac{de}{dt} = -k \cdot |e|^{\alpha} \cdot \text{sign}\,(e) + w, \frac{1}{2}\frac{de^2}{dt} < -k \cdot |e|^{\alpha} \cdot (|e|^{\alpha} - w_0/k). \tag{46}$$

When there is $|e|^{\alpha} > w_0/k$, there is $de^2/dt < 0$. Therefore, when the steady-state error of the system is less than $(w_0/k)^{1/\alpha}$, $0 < \alpha < 1$, the steady-state error of nonlinear feedback control will be reduced exponentially compared with linear feedback control.

In the nonlinear error feedback system, its dynamic process is fal, $a > 0$. This formula has a general solution:

$$e(t) = \begin{cases} \text{sign}\,(e_0) \cdot \left(|e_0|^{1-\alpha} + (1-\alpha)kt\right)^{1/1-\alpha}, \alpha > 1 \\ e_0 \cdot e^{-kt}, a = 1 \\ \text{sign}\,(e_0) \cdot \left(|e_0|^{1-\alpha} + (1-\alpha)kt\right)^{1/1-\alpha}, \alpha < 1, t \le \dfrac{|e_0|^{1-\alpha}}{k \cdot (1-\alpha)} \end{cases}. \tag{47}$$

When α takes different values, we can get

$\alpha > 1$ time, Error to$1/(kt)^{1/(\alpha-1)}$ Velocity attenuation of ;

$\alpha = 1$ time, Error to$1\ e^{-kt}$ Exponential decay of velocity ;

$\alpha < 1$ time, stay $t = |e_0|^{1-\alpha}/k \cdot (1-\alpha)$ At time, the error attenuation decreases to 0 in a finite time, which is a finite time attenuation. (48)

$u = -k \cdot |e|^{\alpha} \cdot \text{sign}\,(e)$ is called nonsmooth feedback when there is $0 \le \alpha < 1$.

Figure 2 shows the structure diagram of the second-order ADRC controller. Among them, v_0 is the system given, x_1 is the transition process arranged by the tracking differentiator, and x_2 is the differentiation of x_1. After "compensation", the control variable u finally acts on the controlled object, y is the actual output of the system, and w is the synthesis of various "disturbances" in the system. The "error integral" feedback is no longer required here. The significance of ADRR lies in the compensation term $-z_3(t)/b$.

To sum up, we can get the design method of ADRC, namely "ADRC algorithm". Since the actual control is realized by a microprocessor.

In this case, for any switching signal satisfying (29), the filter error system is GUES. If -0 in the initial state of 0, $\Omega \le 0$,

$$\begin{aligned} \Omega = & \sum_{t_\theta = t_0}^{t_{i-1}} \mu_i^{N(t_\theta, t_0)} \nu_i^{T_i(t_\theta, t_0)} \\ & \times \exp\left(-a_{i,0}\theta_{a_{i,0}}(t_\theta, t) - a_{i,1}\theta_{a_{i,1}}(t_\theta, t) + \beta_{i,0}\theta_{\beta_i}(t_\theta, t)\right) \\ & \times \int_{t_\theta}^{t_\theta+1} \exp\left(-a_{i,0}\breve{T}_i - a_{i,1}\widehat{T}_i + \beta_i\tilde{T}_i\right)\Gamma(s)ds \le 0, \\ & \sum_{t_\theta = t_0}^{t_{i-1}} \int_{t_\theta}^{t_\theta+1} \mu_i^{N(t_\theta, t)} \nu_i^{T_i(t_\theta, t)} \times esp\left(-a_{i,0}\breve{T}_i - a_{i,1}\widehat{T}_i + \beta_i\tilde{T}_i\right)\Gamma(s)ds \le 0. \end{aligned} \tag{49}$$

So, there are

$$\sum_{t_\theta=t_0}^{t_{i-1}}\int_{t_\theta}^{t_\theta+1}\mu_i^{N(t_\theta,t)}\nu_i^{T_i(t_\theta,t)}\times\exp\left(-a_{i,0}\breve{T}_i-a_{i,1}\hat{T}_i+\beta_i\tilde{T}_i\right)e^T(s)e(s)ds\le$$
$$\sum_{t_\theta=t_0}^{t_{i-1}}\int_{t_\theta}^{t_\theta+1}\gamma^2\mu_i^{N(t_\theta,t)}\nu_i^{T_i(t_\theta,t)}\times\exp\left(-a_{i,0}\breve{T}_i-a_{i,1}\hat{T}_i+\beta_i\tilde{T}_i\right)\omega^T(s)\omega(s)ds. \tag{50}$$

Notice that $\breve{T}_i/\tau_i \le T_i/\tau_i$, and $0 \le N(t_\theta, t) \le T_i/\tau_i$, $T_i = t - t_\theta$, So there are:

$$\begin{aligned}
&\sum_{t_\theta=t_0}^{t_{i-1}}\int_{t_\theta}^{t_\theta+1}\mu_i^{T_i/\tau_i}\nu_i^{\breve{T}_i/\tau_i}\times\exp\left(-a_{i,0}\breve{T}_i-a_{i,1}\hat{T}_i+\beta_i\tilde{T}_i\right)e^T(s)e(s)ds\le\\
&\sum_{t_\theta=t_0}^{t_{i-1}}\int_{t_\theta}^{t_\theta+1}\mu_i^{T_i/\tau_i}\nu_i^{\breve{T}_i/\tau_i}\times\exp\left(-a_{i,0}\breve{T}_i-a_{i,1}\hat{T}_i+\beta_i\tilde{T}_i\right)\gamma^2\omega^T(s)\omega(s)ds\\
&\sum_{t_\theta=t_0}^{t_{i-1}}\int_{t_\theta}^{t_\theta+1}\exp\left((T_i/\tau_i)\ln\mu_i+\left(\breve{T}_i/\tau_i\right)\ln\nu_i-a_{i,0}\breve{T}_i-a_{i,1}\hat{T}_i+\beta_i\tilde{T}\right)e^T(s)e(s)ds\le\\
&\sum_{t_\theta=t_0}^{t_{i-1}}\int_{t_\theta}^{t_\theta+1}\exp\left((T_i/\tau_i)\ln\mu_i+\left(\breve{T}_i/\tau_i\right)\ln\nu_i-a_{i,0}\breve{T}_i-a_{i,1}\hat{T}_i+\beta_i\tilde{T}_i\right)\gamma^2\omega^T(s)\omega(s)ds
\end{aligned} \tag{51}$$

$$\begin{aligned}
&\sum_{t_\theta=t_0}^{t_{i-1}}\int_{t_\theta}^{t_\theta+1}\exp\left(\breve{T}_\theta\breve{\eta}+\hat{T}_\theta\hat{\eta}+\tilde{T}_\theta\tilde{\eta}\right)e^T(s)e(s)ds\le\sum_{t_\theta=t_0}^{t_{i-1}}\int_{t_\theta}^{t_\theta+1}\exp\left(\breve{T}_\theta\breve{\lambda}+\hat{T}_\theta\hat{\lambda}+\tilde{T}_\theta\tilde{\lambda}\right)\gamma^2\omega^T(s)\omega(s)ds\\
&\sum_{t_\theta=t_0}^{t_{i-1}}\int_{t_\theta}^{t_\theta+1}\exp\left(\eta(t-s)\right)e(s)ds\le\sum_{t_\theta=t_0}^{t_{i-1}}\int_{t_\theta}^{t_\theta+1}\exp\left(\lambda(t-s)\right)\gamma^2\omega^T(s)\omega(s)ds.
\end{aligned} \tag{52}$$

So we get

$$\int_{t_0}^{t}\exp\left(\eta(t-s)\right)e^T(s)e(s)ds\le\int_{t_0}^{t}\exp\left(\lambda(t-s)\right)\gamma^2\omega^T(s)\omega(s)ds. \tag{53}$$

Obviously, inequality (50) can be transformed into inequality (51):

$$\int_0^{\infty}\exp\left(\eta(t-s)\right)e^T(s)e(s)ds\le\int_0^{\infty}\exp\left(\lambda(t-s)\right)\gamma^2\omega^T(s)\omega(s)ds, \tag{54}$$

get $\eta < \lambda$, and

$$\begin{aligned}
&\int_0^{\infty}\exp\left(\eta(t-s)\right)e^T(s)e(s)ds\le\int_0^{\infty}\exp\left(\lambda t-\eta s\right)e^T(s)e(s)ds,\\
&\int_0^{\infty}\exp\left(-\eta s\right)e^T(s)e(s)ds\le\int_0^{\infty}\exp\left(-\lambda s\right)\gamma^2\omega^T(s)\omega(s)ds,\\
&\int_0^{\infty}\exp\left(-(\eta-\lambda)s\right)e^T(s)e(s)ds\le\int_0^{\infty}\gamma^2\omega^T(s)\omega(s)ds.
\end{aligned} \tag{55}$$

Among, $\epsilon = \eta - \lambda$。.

2.4. Active Disturbance Rejection Control Strategy of Induction Motor. The entire induction motor control system can be decomposed into two subsystems: flux linkage and rotational speed. Due to the influence of the coupling effect, the flux link will interact, and the dynamic performance of the induction motor is inevitably affected. The mutual coupling between the flux link and the speed loop and the model disturbance caused by the parameter change can be treated as the disturbance of the system. We use the decoupled control variable u_{sd}, u_{sq} to decouple the rotation speed ω_r of the flux linkage Ψ_{rd}, respectively.

The design of the speed loop ADR controller The mathematical model of the induction motor speed loop is

$$\dot{\omega}_r = k\cdot\psi_{rd}\cdot i_{sq}-w_l(t). \tag{56}$$

Among them, there is $w_1(t) = -P_n \cdot T_L/J$.

Both the load torque T_L and the moment of inertia J will change with different working conditions to form unknown disturbances. In the actual operation process, the variation range is large, which has a great influence on the speed performance. According to the characteristics of ADRC, $w_I(t)$ can be regarded as an unknown disturbance, which can be compensated by real-time estimation of the extended

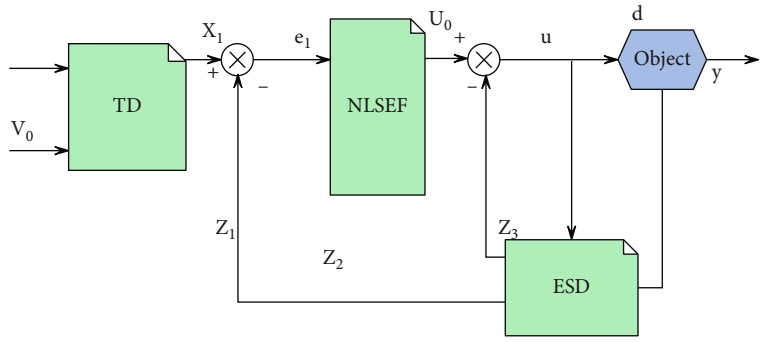

Figure 3: ADRC controller structure diagram.

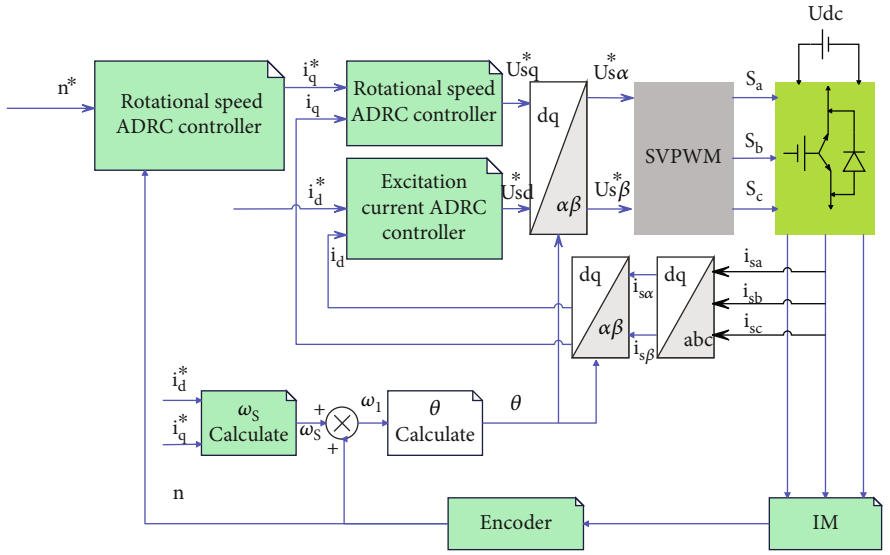

Figure 4: Induction motor vector control system based on active disturbance rejection control.

observer. A first-order ADRC control of the speed loop is considered, and its structure is shown in Figure 3.

The corresponding first-order ADRC controller equation is

$$
\begin{aligned}
TD:&\begin{cases} x_1(k+1) = x_1(k) + T \cdot x_2(k), \\ x_2(k+1) = x_2(k) + T \cdot fst(x_1(k) - u(k), x_2(k), r, h), \end{cases} \\
ESO:&\begin{cases} \varepsilon(k) = z_l(k) - \omega_r(k), \\ z_l(k+l) = z_l(k) + T \cdot (z_2(k) - \beta_1 \cdot \mathrm{fal}(\varepsilon(k), \alpha_l, \delta_l) + b \cdot u(k)), \\ z_2(k+l) = z_2(k) - T \cdot \beta_2 \cdot \mathrm{fal}(\varepsilon(k), \alpha_l, \delta_1), \end{cases} \\
NLSEF:&\begin{cases} e_l(k) = x_1(k) - z_l(k), \\ u_0(k) = \beta_3 \cdot fal(e_l(k), \alpha_2, \delta_2), \\ u(k) = u_0(k) - z_2(k)/b. \end{cases}
\end{aligned} \tag{57}
$$

In ESO, z_2 can well estimate disturbance $w_1(t)$ and some unmodeled disturbances, and in NLSEF, we compensate the control signal of the system, so that the speed of induction motor can be approximately simplified to a first-order linear object. It realizes the mathematical fitting of the empirical knowledge of the control engineering field "large error, small gain, small error, large gain" through nonlinear feedback, which improves the dynamic performance and robustness of the ADRC.

The mathematical model of the q-axis current loop of the induction motor is

$$\dot{i}_{sq} = -k \cdot i_{sq} + w_2(t) + \frac{1}{\sigma} \cdot u_{sq}. \tag{58}$$

Among them, there is $w_2(t) = -L_m/\sigma \cdot L_r \cdot \psi_{rd} \cdot \omega_r - i_{sd} \cdot \omega_e$.

Therefore, the current loop still adopts the first-order ADRC, and its design is similar to the speed loop.

The mathematical model of the d-axis current loop of the induction motor is

$$\dot{i}_{sd} = -k \cdot i_{sd} + w_3(t) + u_{sd}/\sigma. \tag{59}$$

Among them, there is $w_3(t) = k \cdot \psi_{rd} + i_{sd} \cdot \omega_e, k = R_r \cdot L_m/\sigma \cdot L_r^2$.

The coupling term formed by i_{sd}, w_e and the variable motor parameters such as rotor resistance R_r exist in

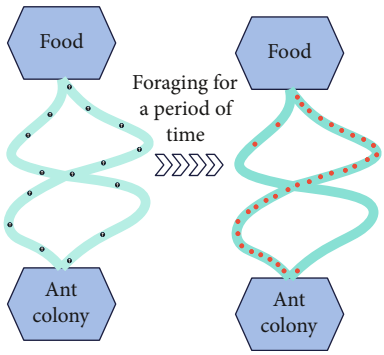

Figure 5: Foraging process of ant colony.

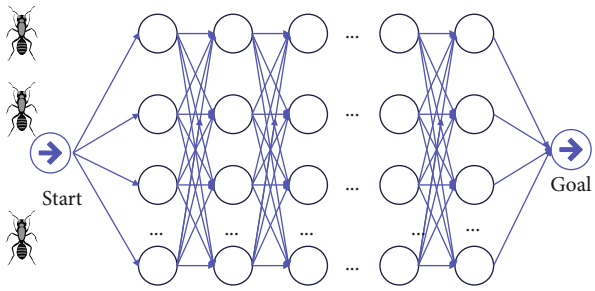

Figure 6: Traditional optimization diagram.

disturbance $w_3(t)$, which can be estimated by ESO and compensated. According to the mathematical model of the d-axis current loop, a first-order ADRC is established to control the d-axis current, thereby indirectly controlling the flux linkage.

The active disturbance rejection loop controller is used as the given i_q^* of the torque current. The three-phase current i_a, i_b, i_c of the induction motor stator detected by the current sensor is transformed by $3s/2s$ to obtain the two-phase static current i_α, i_β, and then transformed by $2s/2r$ to obtain the currents i_d and i_q in the two-phase rotating coordinate system. The error between i_d and i_q and the given current is input into the active disturbance rejection controller, and its output is U_d, U_q, U_d, U_q, and the inverter output applies the DC bus voltage U_{dc} to the induction motor in the form of PWM waves. Control system based on active disturbance rejection control is shown in Figure 4.

The multi-Lyapunov energy function method is used and its expression is given. By giving each subsystem its corresponding energy function, instead of describing the energy states of all subsystems with one energy function, the conservatism of the conclusion can be greatly reduced and it is closer to the actual engineering situation. Then, for the complex asynchronous situation, under the assumption that multiple asynchronous time periods may overlap with each other, the mathematical model is first given. After stability analysis and proof, the model-dependent residence time criterion for the global asymptotically consistent stability of the event-triggered switching system is obtained.

Considering that the existing conclusions are partly based on the minimum dwell time, it is highly conservative. Therefore, in this paper, studying the stability of event-triggered switching systems based on the model-dependent residence time criterion reduces the conservativeness of the conclusions. Compared with other residence time criteria, the residence time of each subsystem described by the model-dependent residence time is different, and it is determined according to the characteristics of each subsystem, which greatly increases the flexibility of switching rules. At the same time, this criterion is closer to actual engineering. In actual engineering, for a switching system, it is difficult to guarantee the residence time of each subsystem.

2.5. Active Disturbance Rejection Control Strategy of Induction Motor Based on Ant Colony Algorithm. Active disturbance rejection control of induction motor is the main method to reduce the noise of electrical automation control system. In this paper, the ant colony algorithm in the simulation algorithm is selected as the basis for modeling, and the detailed analysis is given below.

The optimization process of the ant colony is shown in Figure 5.

Ant colony algorithm is a metaheuristic algorithm proposed in the background of ant foraging behavior, as shown in Figure 6. Ant colony algorithm is to find the optimal solution for the problem to be optimized among all the feasible solutions that constitute the problem to be optimized.

These nodes will appear in the form of node sequences. If the k-th ant is at node i, it will select the next node j according to the probability $P_k(i,j)$.

$$P_k(i,j) = \begin{cases} \dfrac{\tau^\alpha(i,j)\cdot\eta}{\beta_{(}(i,j)}, & \\ \displaystyle\sum_{j\in N_i^k} \tau_{(i,j)\cdot\eta}\beta_{(i,j)}, & \text{When } j \in N_i^k, \\ 0, & \text{other.} \end{cases} \tag{60}$$

Among them, N_i^k represents all the node sets that can be selected, $\eta(i,j)$ is an independent function $\eta(i,j) = 1/f(X)$ that needs to be minimized, and $f(X)$ is the value of the cost equation X. Ants will release pheromone on the path they pass through, which is calculated by the following formula:

$$\tau_k(i,j) = \begin{cases} \dfrac{Q}{Y_k}, & \text{If the kth ant goes from node i to node j} \\ 0, & \text{otherwise} \end{cases} \tag{61}$$

Among them, Q is the constant of the total amount of pheromone released by each ant, and Y_k represents the pros and cons of the k-th ant's optimization result. In the transition probability law, each ant uses both visibility information and pheromone density to select nodes. The visibility information $\eta(i,j)$ and the pheromone density $\tau(i,j)$ represent the pros and cons of the ant located at the node i taking the node j as the next node to pass through. The visibility

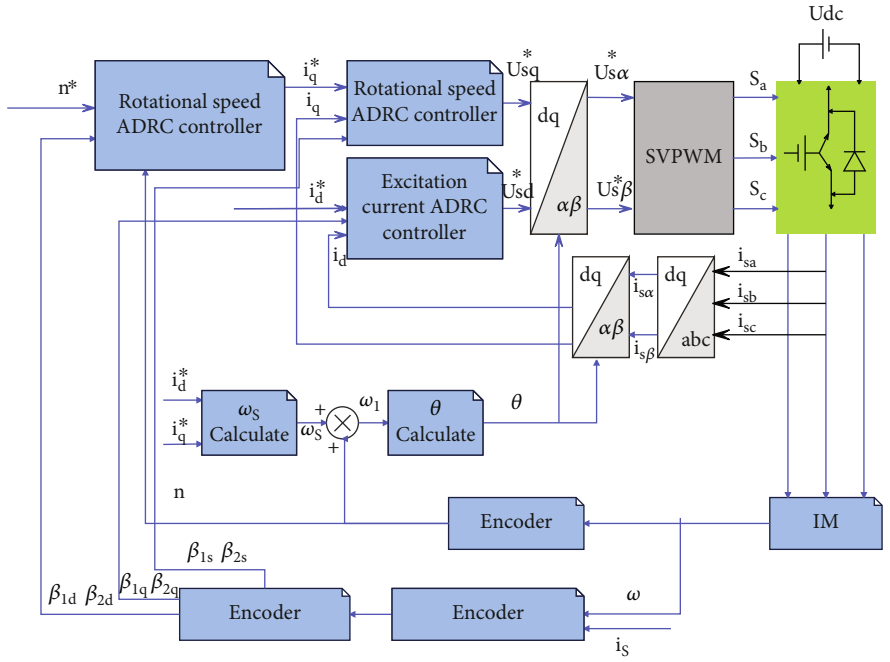

Figure 7: Structure diagram of ADRC control of induction motor based on ant colony algorithm.

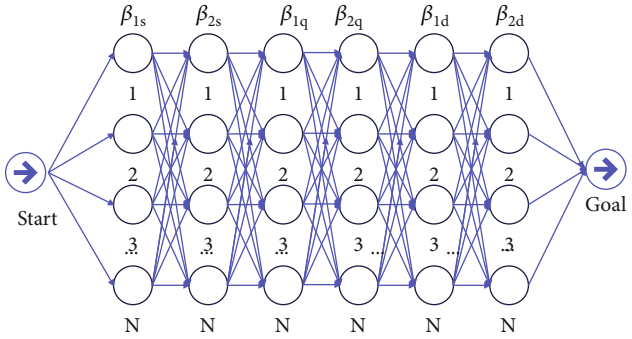

Figure 8: Parameter optimization range of traditional optimization graph.

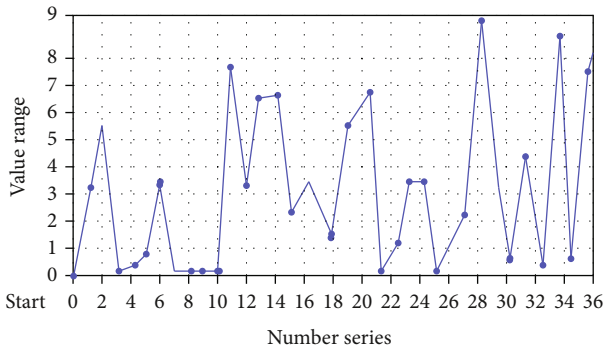

Figure 9: Parameter optimization range of the new optimization graph.

Table 1: The effect of electrical automation control system based on intelligent computer algorithm.

Number	Electrical control	Number	Electrical control	Number	Electrical control
1	87.52	12	88.38	23	90.64
2	88.39	13	91.84	24	83.46
3	84.18	14	84.33	25	83.96
4	88.97	15	86.04	26	86.98
5	89.08	16	86.33	27	83.16
6	87.87	17	88.57	28	89.78
7	86.92	18	87.64	29	91.09
8	83.04	19	90.42	30	83.95
9	90.12	20	91.95	31	91.21
10	89.61	21	90.93	32	91.98
11	85.92	22	89.45	33	86.94

information $\eta(i, j)$ is generated by a function independent of the optimization problem itself, but the pheromone density comes from the good optimization results produced by the ant. Therefore, the transition probability law is the embodiment of the trade-off between the node visibility and the pheromone density.

When all the ants complete their respective paths, it is called the ant colony algorithm completes an iterative operation. At this time, the pheromone density value of the node will be calculated according to the pheromone update law, which is used to update the pheromone amount on the path passed by the ant colony before.

$$\tau_{M+l}(i, j) = (1 - \rho) \times \tau_M(i, j) + \sum_{k=1}^{m} \tau_k(i, j). \quad (62)$$

Among them, m represents the number of ants in the ant colony, M represents the number of iterations of the ant colony algorithm that has been carried out, ρ is the pheromone

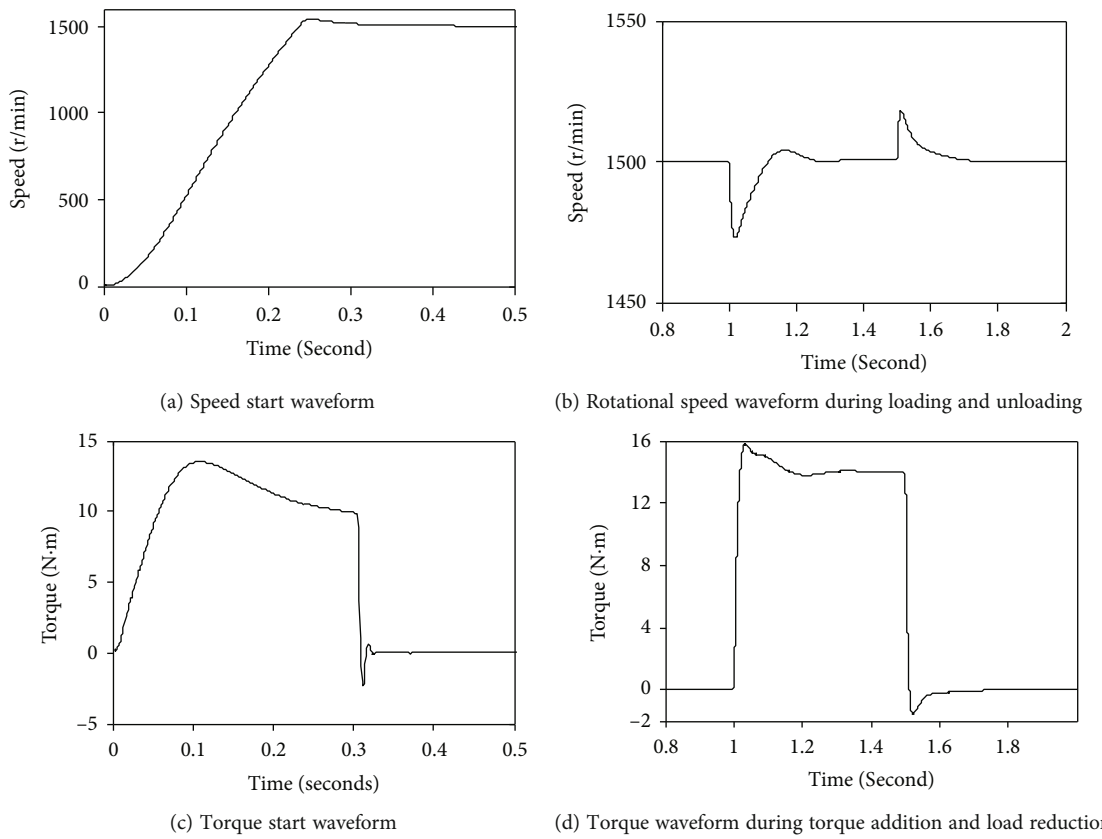

(a) Speed start waveform

(b) Rotational speed waveform during loading and unloading

(c) Torque start waveform

(d) Torque waveform during torque addition and load reduction

Figure 10: Verification of correctness of active disturbance rejection control.

volatilization rate, $\rho \in (0, 1)$. Therefore, $1 - \rho$ represents the residual rate of the pheromone after volatilization from the M-th iterative calculation to the $M+1$-th iterative calculation. In the pheromone update law, the pheromone on the path passed by the ants is volatilized in the next iterative calculation by the pheromone volatilization rate ρ. In other words, the pheromone update law is to obtain more pheromone accumulation on the optimal solution.

In this paper, control structure is shown in Figure 7.

The ant colony algorithm is the active disturbance rejection controller parameters. In the ant colony active disturbance rejection control strategy, according to the feedback results of the controlled object, the ant colony algorithm completes the parameter optimization, forms a feedback mechanism, and enhances the robustness of the control system, as shown in Figure 8).

2.6. Ant Colony Algorithm Objective Function Model. The parameters of the ant colony algorithm are shown in Table 1, and the parameters m, M, $M0$, α, β, and ρ are set to initial values.

The ant selects a node according to the probability of the node being selected as the next node to reach, until the ant reaches the end point, all the selected nodes constitute a path. The probability of a node being selected is calculated according to the following formula:

$$P(i,j) = \frac{\tau^{\alpha}(i,j) \cdot \eta^{\beta}(i,j)}{\sum_{j=0}^{9} \tau^{\alpha}(i,j) \eta^{\beta}(i,j)}. \tag{63}$$

When k ants reach the end point, the update amount of pheromone on the node selected by them will be calculated, and the update amount of pheromone will be calculated. Among them, Yk represents the quality of the optimization result

$$\Delta\tau_k(i,j) = \begin{cases} \dfrac{Q}{Y_k}, & \text{if the } k\text{th ant passes through the node (i, j)}, \\ 0, & \text{other.} \end{cases} \tag{64}$$

When all m ants are optimized, the pheromone on each node will be updated as follows:

$$\begin{aligned} \tau_{M+1}(i,j) &= (1-\rho) \cdot \tau_M(i,j) + \Delta\tau(i,j), \\ \Delta\tau(i,j) &= \sum_{k=1}^{m} \tau_k(i,j). \end{aligned} \tag{65}$$

The updated pheromone amount of each node will affect the node selection of the ants in the next optimization of the ant colony.

The method of determining the visibility of a node is as follows:

$$\eta(i,j) = \frac{10 - \left| y_j - y_j^{*} \right|}{10}. \tag{66}$$

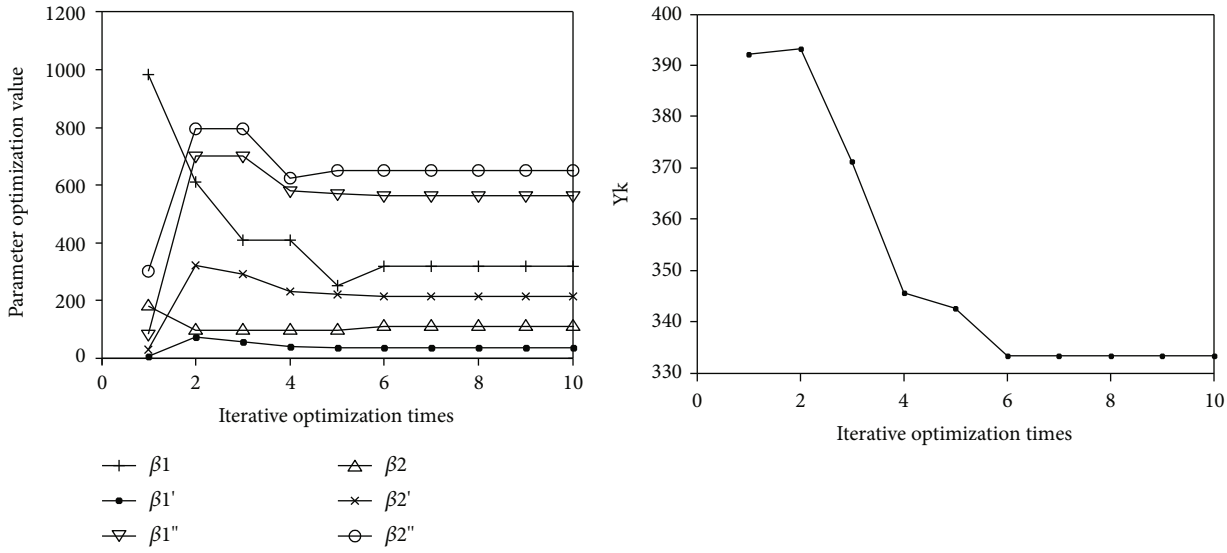

(a) Parameter convergence curve

(b) Objective function convergence curve

Figure 11: Verification of the convergence of ant colony active disturbance rejection.

Table 2: Parameter meaning of ant colony algorithm.

Parameter	Meaning
m	The number of ants in the colony
M	The maximum number of optimizations of the ant colony
M0	The number of optimizations performed by the ant colony
Q	Constant coefficient
α	Pheromone importance factor
β	Heuristic function importance factor
ρ	Pheromone volatile factor
$\tau(i, j)$	Pheromone value at node (i, j)
$\eta(i, j)$	The expected degree of node (i, j) being selected $P(i, j)$; the probability that node (i, j) is selected
Yk	The objective function value of the kth $(k = 1, 2 \cdots m)$ ant

In the formula, yj represents the parameter value generated in this optimization, and y_j^* represents the parameter value corresponding to the generated optimal solution.

3. Effect Verification of Electrical Automation Control System Based on Intelligent Computer Algorithm

This paper builds an intelligent simulation model, the main research goal of this paper is to study the control effect of the control system, and then analyze the system performance through system simulation.

Next, this paper verifies the effect of the electrical automation control system based on the intelligent computer algorithm proposed in this paper, and counts the electrical automatic control simulation effect of the model in this paper. In order to simplify the calculation amount of ant colony algorithm and improve the calculation accuracy, this paper studies a new optimization graph, and the optimization result is shown in Figure 9.

Figure 10 shows the speed and torque waveforms of sudden addition and sudden load shedding when the ADRC system starts from no-load to the rated speed of 1500 r/min. Among them, the load torque changes from no-load to rated load at 1 s, and suddenly decreases to no-load at 1.5 s. From the simulation results, it can be seen that the ADRC system has good performance in both dynamic and static conditions.

In Figure 11, after 6 iterations of the ant colony algorithm, the parameters no longer change, and the objective function Yk reaches the minimum value, indicating that the parameter optimization has achieved the optimal result, and the corresponding parameter group is the optimal solution. The ant colony active disturbance rejection control strategy can automatically optimize the parameters and approach the optimal solution successively by iterative operation. Therefore, due to the self-learning ability of the ant colony algorithm, the optimal performance will be finally obtained through the iterative operation.

The effect of the electrical automation control system based on the intelligent computer algorithm proposed in this paper is counted, and the results shown in the following Table 2 are obtained.

It can be seen from the above research that the electrical automatic control system based on the intelligent computer algorithm proposed in this paper has a good electrical automatic control effect.

4. Conclusion

In recent years, the research on collaborative planning of electrical interconnection systems has just begun, and there are still many problems that need further research. How to

consider the mutual conversion and influence mechanism of electric load and gas load in the process of planning and operation, how to coordinate the independence of decision-making of different energy market entities during planning and operation, and how to deal with the uncertain factors caused by the independence of decision-making. In addition to hardware, there are electrical automation software and electrical automation systems. In order to improve the effect of electrical automation control, this paper combines the intelligent computer technology to construct the electrical automation control system. The research shows that the electrical automatic control system based on the intelligent computer algorithm proposed in this paper has a good electrical automatic control effect.

Data Availability

The labeled dataset used to support the findings of this study are available from the corresponding author upon request.

Conflicts of Interest

The author declares no competing interests.

Acknowledgments

This study is sponsored by the Xinyang Vocational and Technical College.

References

[1] Y. Zuo, X. Zhu, L. Quan, C. Zhang, Y. Du, and Z. Xiang, "Active disturbance rejection controller for speed control of electrical drives using phase-locking loop observer," *IEEE Transactions on Industrial Electronics*, vol. 66, no. 3, pp. 1748–1759, 2019.

[2] M. K. A. A. Rahim, M. H. Zahari, M. F. F. Rahimi, and Z. M. Amin, "Home automation controller with security system," *Multidisciplinary Applied Research and Innovation*, vol. 3, no. 1, pp. 475–481, 2022.

[3] D. M. N. Bristol, E. J. B. Agustin, and H. A. Alcaraz, "Bibliometric analysis on the application of electro-pneumatic control system as automation technology," *International Journal of Progressive Research in Science and Engineering*, vol. 3, no. 4, pp. 60–67, 2022.

[4] S. Zinchenko, V. Mateichuk, P. Nosov et al., "Use of simulator equipment for the development and testing of vessel control systems," *The Scientific Journal of Riga Technical University-Electrical, Control and Communication Engineering*, vol. 16, no. 2, pp. 58–64, 2020.

[5] C. Gehrmann and M. Gunnarsson, "A digital twin based industrial automation and control system security architecture," *IEEE Transactions on Industrial Informatics*, vol. 16, no. 1, pp. 669–680, 2020.

[6] Y. Bichiou and H. A. Rakha, "Developing an optimal intersection control system for automated connected vehicles," *IEEE Transactions on Intelligent Transportation Systems*, vol. 20, no. 5, pp. 1908–1916, 2019.

[7] K. Eltag, M. S. Aslamx, and R. Ullah, "Dynamic stability enhancement using fuzzy PID control technology for power system," *International Journal of Control, Automation and Systems*, vol. 17, no. 1, pp. 234–242, 2019.

[8] K. Wang, E. Tian, J. Liu, L. Wei, and D. Yue, "Resilient control of networked control systems under deception attacks: a memory-event-triggered communication scheme," *International Journal of Robust and Nonlinear Control*, vol. 30, no. 4, pp. 1534–1548, 2020.

[9] M. Saraswat, K. Sharma, N. R. Chauhan, and R. K. Shukla, "Role of automation in energy management and distribution," *Journal of Scientific and Industrial Research (JSIR)*, vol. 79, no. 10, pp. 951–954, 2020.

[10] D. Xu, B. Wang, G. Zhang, G. Wang, and Y. Yu, "A review of sensorless control methods for AC motor drives," *CES Transactions on electrical machines and systems*, vol. 2, no. 1, pp. 104–115, 2018.

[11] M. Dumitrescu, "Marine industry automation systems simulation," *Scientific Bulletin" Mircea cel Batran" Naval Academy*, vol. 22, no. 2, pp. 7–13, 2019.

[12] H. Chen, B. Jiang, and N. Lu, "A multi-mode incipient sensor fault detection and diagnosis method for electrical traction systems," *International Journal of Control, Automation and Systems*, vol. 16, no. 4, pp. 1783–1793, 2018.

[13] B. Pratap and S. Purwar, "Real-time implementation of nonlinear state and disturbance observer-based controller for twin rotor control system," *International Journal of Automation and Control*, vol. 13, no. 4, pp. 469–497, 2019.

[14] Y. Yuan, H. Yuan, D. W. Ho, and L. Guo, "Resilient control of wireless networked control system under denial-of-service attacks: a cross-layer design approach," *IEEE transactions on cybernetics*, vol. 50, no. 1, pp. 48–60, 2020.

[15] S. J. Gambhire, D. R. Kishore, P. S. Londhe, and S. N. Pawar, "Review of sliding mode based control techniques for control system applications," *International Journal of dynamics and control*, vol. 9, no. 1, pp. 363–378, 2021.

[16] O. V. Kryukov, I. V. Gulyaev, and D. Y. Teplukhov, "Method for stabilizing the operation of synchronous machines using a virtual load sensor," *Russian Electrical Engineering*, vol. 90, no. 7, pp. 473–478, 2019.

[17] M. S. Jansi and M. K. Elaiyarani, "IOT based home automation system," *Turkish Journal of Computer and Mathematics Education (TURCOMAT)*, vol. 11, no. 3, pp. 2246–2253, 2020.